Hybrid auxetic foam and perforated plate composites for human body support

H. Mohanraj[1], S L M Filho Ribeiro[2], T. H. Panzera[2], F. Scarpa[1], I. R. Farrow[1], R. Jones[3], A. Davies-Smith[3], C. D.L. Remillat[1], P. Walters[4], H-X Peng[5]

[1]Advanced Composites Centre for Innovation and Science (ACCIS), University of Bristol, BS8 1TR Bristol, UK
[2]Centre for Innovation and Technology in Composite Materials, Department of Mechanical Engineering, Federal University of São João del Rei, Brazil
[3]MS Research, Treatment & Education, The Vassall Centre, Gill Avenue, Bristol BS16 2QQ
[4]Centre for Fine Printing Research (CFPR), University of the West of England, Bristol School of Art and Design, Bower Ashton Campus, Bristol BS3 2JT UK
[5]Institute for Composites Science Innovation, School of Materials Science and Engineering, Zhejiang University, Hangzhou, 310027, PR China

Abstract

The paper describes the design, manufacturing, modelling and testing of a hybrid composite support made from auxetic open cell foam liners and curved thermoplastic plates with rhomboidal perforations for human body support. Both the foam and the curved perforated plate have in-plane negative Poisson's ratio behaviour. The static bending stiffness of the hybrid auxetic composite support is modelled using an analytical and Finite Element approach benchmarked against experimental results from three-point bending tests. The benchmarked Finite Element models are used to develop a map of optimized static stiffness versus the geometry of the rhomboidal perforations. A Design of Experiment testing campaign is also carried out on sixteen hybrid auxetic composite plates to understand the interaction and correlation of the static bending versus the geometry of the perforations and the contribution given by the auxetic foam liner.

Keywords: auxetic; foam; curved plate; perforations; modelling; testing;

1. Introduction

Multiple sclerosis is a condition that affects the central nervous system of the body [1]. Nearly 75% of MS patients suffer from tremors at some point during their lives [2]. A tremor can be described as a rhythmic, trembling or shaking movement that cannot be controlled voluntarily. Tremor may be experienced as small, shaking movements or as larger movements. If tremor develops, it tends to be some years after the occurrence of the first MS symptoms, typically between five and 15 years [2]. There are primarily two types of tremor caused by MS: a) the Intention Tremor caused during the patients intentional movement and b) the Postural one, occurring when the patient sits or stands [2]. Vibrations caused by tremor can have effects such as: degraded comfort, interference with activities, and impaired health [3]. Horizontal vibration (fore and aft or lateral) vibration of the seated body causes different range of sensations. It has been observed that with vibrations at frequencies between 1Hz-3Hz it is difficult to stabilize the upper part of the body, and the discomfort caused by the vibration acceleration tends to be greatest [3]. The presence of a backrest can help modify the effects of tremor caused horizontal vibrations. At low frequencies the backrest can help stabilize the upper body and reduce the effects of motion, but at high frequencies the backrest can be a primary cause of vibration being transmitted to the torso. Because of the relative low frequency range involved in these motions (1Hz – 10Hz), from a design perspective there is the interest of optimising the stiffness of any type of semi-rigid support that could be used to stabilize the patient. The simplest backrest/support is made out of perforated fabric and nylon straps. These supports have been used on office hairs to reduce the effect of fatigue to the back by providing comfort, although they are not capable of reducing the high amplitude vibrations caused by MS induced tremors. Special backrests are placed on wheel chairs to provide extra support and comfort. Aforementioned backrests are generally good for static and for lower frequency tremors but with the increase in frequency of vibration (10 Hz) the backrest can increase the effect of the tremor [3][4]. The backrest can be highly rigid and once the torso is not in contact can be ineffective. Support vests have been developed to support and mainly correct the posture. These vests cling on to the torso and can provide constraints to correct the posture [5]. Currently these support vests are generally used to help individuals to recover from injuries to their back. Although these vests provide support they can't reduce the effects of tremors. Furthermore they can be uncomfortable and reduce mobility for an MS patient. All these factors make it apparent that a support that makes better use of the support material and provides tailored support during tremors could constitute a significant device to alleviate discomfort and improve posture for MS patients or, more in general, wheelchair-bound patients.

Auxetic materials feature characteristics such as uniform repartition of stresses, adaptability to different shapes and are evaluated in applications in which shock absorption is of importance. Auxetic materials have improved indentation resistance, enhanced bending stiffness in structural elements and shear compliance in comparison to their conventional counterparts [6]-[13]. Auxetic behaviour has also been shown to exist with a number of materials; silicates and zeolites, metals, foams and polymers [14][15], whilst utilising a range of different mechanisms; re-entrant units [16][17], rotating square models [18][19][20][21][22][23], chiral systems [24][25][26][27], auxetic composites [28][29], perforated systems with void filled/unfilled with another phase [30] and auxetic behaviour induced by an elastic instability [31]. Foams in particular have provided experimental evidence of high energy absorption under cyclic and impact loading, all characteristics that combined with the sinclastic curvature deformation make negative Poisson's ratio foams appealing materials for sport and biomedical applications [9], [32]-[40].

The paper describes the design and testing of a hybrid auxetic foam/perforated plate structure for human body support. The foam lining is constituted by auxetic foam produced according the manufacturing parameters described in [39][41]. The negative Poisson's ratio foam is applied to a curved flexible support characterised by perforations of rhomboidal shape (see Figure 1 and reference [18]). The use of perforation patterns allows the production of plate-like structures with in-plane auxetic behaviour, and constitutes a relatively novel and inexpensive technique to induce negative Poisson's ratio behaviour in solids [42][43][44]. The hybrid auxetic support is subjected to bending tests through an analysis of variance (ANOVA) to explore the design space of the component, and a Finite Element simulation is carried out to identify a map relating the dimensions of the rhomboidal perforation versus the optimized stiffness of the plate.

2. Manufacturing and testing of the plates and the auxetic foam layer

Four sets of plates were manufactured with ABS plastics and water-cutting techniques (Flow Mach 1) with the geometry parameters listed in Table 1. The separation distances $\boldsymbol{S}$ (10 mm to 15 mm) and perforation dimensions $\boldsymbol{a}$ (15 mm to 35 mm) were chosen based on an initial exploration of the design envelope based on manufacturing constraints and overall size of the plates [19] (see Figure 2). The Poisson's ratio values were previously measured and ranged between -0.7 to -0.2 [19], in agreement with the figures calculated by Grima and Gatt [18]. The working pressure for the water-jet cutting was 55000 psi, with a jet size of +- 1.15 mm, accuracy of ±0.127 mm per 1m and speed of 101.6 mm/min. The plates were curved via a heat forming in an oven at 155^{o}C with the addition of a vacuum bag on a semi-cylindrical tool of 800mm in diameter and 300 mm of height. The foam was manufactured following the thermoforming process described in [39][41] from a single layer of

open cell polyurethane conventional foam (Cardiff Upholstery Ltd, Cardiff - density of 27 kgm^{-3}, hardness 150). The conventional foam was treated under pressure (2 MPa) and temperature (125 ^{o}C) in an autoclave [39] for 20 minutes. The foam with its vacuum bag and half-mould has been cooled in a water bath with running water after the cure time for 25 minutes to obtain the auxetic open cell foam with an average thickness of 10 mm (Figure 3). The surface of the foam mats prepared in this way was 0.7 m^2.

A full factorial design (2^3) and an Analysis of Variance (ANOVA) were used to assess from the experimental point of view for the treatment of the data and analysis of the results. The experimental factors investigated within the Design of Experiment process were the dimensions of the perforations, their separation and the presence (or not) of the auxetic foam layer. The DoE was performed with a 95% confidence level. The mechanical response of the analysis was based on the radial stiffness, which can be estimated by applying Castigliano's Theorem by modifying a formulation proposed by Xiong et al [43] that describes the central displacement in a simply supported curved composite sandwich shell when subjected to a concentrated force. The central displacement δ during the central force F can be expressed as:

$$\delta = \frac{FR}{(EA)_{eq}} f_1(\alpha) + \frac{FR^3}{(EI)_{eq}} f_2(\alpha) \quad (1)$$

Where the functions f_1 and f_2 are dependent upon the semi-arc angle α from the vertical axis of the reference system (see Figure 4) described by the curved beam:

$$f_1(\alpha) = \frac{1}{2\pi}(\sin\alpha)^2 + \frac{1}{4\pi^2}\sin 2\alpha - \frac{1}{16}\sin 2\alpha + \frac{\alpha}{2\pi^2} + \frac{\alpha}{8} \quad (2)$$

$$f_2(\alpha) = \frac{\alpha}{8} - \frac{\sin 2\alpha}{16} + \frac{\alpha}{2\pi^2} + \frac{\sin 2\alpha}{4\pi^2} + \frac{(\sin\alpha)^2}{2\pi} + \alpha\left(\frac{1}{2}\sin\alpha + \frac{1}{\pi}\cos\alpha\right)^2 \quad (3)$$

In (1), $(EA)_{eq}$ and $(EI)_{eq}$ stand for the axial and bending stiffness of the curved beam respectively. If the plate is made from an isotropic equivalent material with Young's (flexural) modulus E_p, thickness t and width w (Figure 4), the radial stiffness K can be estimated as:

$$K = \frac{F}{\delta} = \frac{2E_p w t^3}{R(f_1 t^2 + 4R^2 f_2)} \quad (4)$$

Where R is the radius of the curved beam.

To evaluate the flexural modulus of the ABS plastics used during the manufacturing a series of 3-point bending tests following the ASTM D7264 standard (Figure 5a). For the tests an Instron

machine with 1 kN load cell under displacement control and displacement rate of 2 mm/min was used. Curved plates with and without the perforations (and with the auxetic foam layer deposited with a epoxy adhesive film) were subjected to central loading with the edges simply supported on the base plate of the machine (Figure 5b). The tensile machine and the specifications of the loading were the same as used for the ASTM D7264 tests. The 3-point bending tests on the flat ABS specimens were carried out to check any discrepancy between the data of the plastics specified by the producer (nominally between 2.0 GPa – 2.2 GPa), and the flexural modulus of the polymer obtained from extrapolating Eq. (4) for the curved full plates. Equation (4) was also used to estimate the equivalent flexural modulus of the curved perforated structures. Curved plates with no perforation and with/without the auxetic foam layer have also been subjected to the 3-point bending test. The results from these experimental essays have been used to benchmark the limit configurations of the Design of Experiment campaign, as it will be explained later.

A 2^3 Design of Experiments (DoE) was performed to identify the relation between main factors (the hole dimensions and separations and the foam addition as stiffness increase). The interaction of the various factors (4 levels of interactions) was identified with two series of replicates, for a total of 16 samples tested.

3. Finite Element simulations and optimisation

The Finite Element Abaqus 6.10 code was used to perform the numerical simulations, both to compare the experimental results and perform the stiffness optimization. The plate with the auxetic foam was modelled with eight-node 3D type C3D8R elements with three translational degrees of freedom at each node and Hermite interpolation functions, for a total of 29103 elements with the plate having the smaller perforations (64 C). The mesh sizing was determined after a convergence test on the strain energy distribution. The material properties of the plates were ABS plastics. The foam layer was represented by a transversely isotropic material with Young's modulus of 236 kPa and Poisson's ratio of -0.15, corresponding to loading along the through-the-thickness direction [39]. As it will be clear from the comparison between the numerical and FE results, these assumptions were sufficient to simulate in an adequate manner the radial stiffness behaviour of the hybrid plates. The representation of the real boundary conditions that the back of a user can exert on the support can be quite difficult, as it can be evinced from the scan of a low back area in Figure 6a. For the FE simulations the 3-point bending boundary condition similar to the one used in the experimental tests was used, leading to a bending stiffness K proportional to one expected from mixed boundary conditions [46]. The central distributed force (Figure 6b-d) had a resultant of 65 N, similar to static indentation levels existing in chair supports [3][5], although it must be stressed that

no defined data about the exact magnitude of loads exerted during tremor/large dynamic motions are available in open literature to the best of the Authors' knowledge. All the simulations were linear static with no mass relief applied. To explore the design space of the radial stiffness versus the geometry of the perforations, a mathematical model was proposed used analytical method using the CCD arrangement (Box-Wilson Central Composite Design) which is used to adjust a second order response surface model. A genetic algorithm was developed based on the surface response models (RSM) for *K* followed by the NSGA II algorithm being applied. The objective function was used in the search for optimal combination of input variables (perforation dimension and separation). In the computational model the population was 1000 individuals evolving over than 100 interactions, resulting in a total of 100,000 generations. The algorithm was integrated into the software environment between Matlab ™ and Abaqus. The optimization problem was formulated as: Max *f(K)*, Subject to 0.2 (mm) ≤ Hole dimension ≤ 50 (mm) and 0.2 (mm) ≤ Hole separation ≤ 30 (mm).

4. Results and discussions

The experimental flexural modulus obtained through the ASTM three point bending test was found to be 2.06 GPa (standard deviation ~ 3 % of the mean value). This value is very close to the manufacturer's quoted flexural modulus of 2.0 GPa-2.2 GPa, with an error of 6.36%. Using the experimental data for plates with no perforations and no foam it was possible to find the material flexural modulus by back substitution from Equation (4). The value was obtained for R = 400 mm, t = 2 mm, w = 300 mm, $\alpha = 12^{o}$. The value obtained was 2.08 GPa (standard deviation ~ 4% of the average), which suggests that the theoretical model used for the calculation of the bending stiffness of the curved plates provides a more than satisfactory approximation. Since the equation is valid for plates with no perforations it can be applied to curved plates with perforations to estimate the bending stiffness of these hybrid structures. The curved plates with no perforation and no foam had a bending stiffness of 6.57 N/mm. When adding the foam layer, the plates increased the stiffness by 94% (up to 12.8 N/mm).

Figure 7 shows the distribution of the results in terms of normal probability versus residuals. For an effective DoE it is important that the experimental results follow a normal distribution to guarantee the reliability and robustness of the results. It can be seen from Figure 7 that the experimental results follow the normal distribution line closely, and this gives confidence on the quality of the experimental results and the methodology used.

The analysis of variance gives important information about how the three different factors interact with each other and affect the bending stiffness response *K* of the curved plates (Table 2). The P

values analysed give an indication of which factor is the dominant one over the bending stiffness. The analysis was done with a 95% confidence level, hence a P value less or equal to 0.05 (5%) means that factor has a significant effect on *K*. The perforation dimensions affect the stiffness response of the curved plates on their own [18][19]. This phenomenon was confirmed by the DoE analysis, with a resulting P value of 0.000. The addition of the auxetic foam alone also affects the *K* value of the curved plates significantly, with a P value of 0.000. What is interesting to note is that the perforation separation on its own cannot affect *K,* as the P-value calculated is 0.455 and outside the confidence zone. The ANOVA shed light on how the main factors affect *K* alone, but more importantly the analysis showed how the three main factors work together. The P-value for the perforation spacing and perforation dimension interaction (Figure 8) was found to be 0.001, suggesting a significant influence of this interaction over the bending stiffness. With perforation dimensions of 15mm and perforation separations of 10mm a very low bending stiffness is achieved (4 N/mm), but this value can be increased to 5.3 N/mm with the same perforation dimension and using a perforation separation of 15mm. Nearly the same value of *K* can be however achieved with perforation dimensions of 35 mm and a separation of 15mm. The highest bending stiffness is achieved when a perforation dimension of 35mm is combined with a perforation separation of 10mm (6.5 N/mm), nearly the stiffness provided by a curved plate with no perforations and without any auxetic foam. That particular plate has however a large section on the boundary that is not perforated, and may provide a stiffening frame effect on the overall response. The difference between the highest and lowest value of *K* achieved within this interaction is nearly 61%. The interaction between the separation of the perforation and the auxetic foam insert describes a different picture (Figure 9). With a P-value of 0.000 it is apparent that there is significant coupling between the use of the foam and the perforation separation. It is interesting to notice that with a perforation separation of 15 mm and the presence of an auxetic foam it is possible to achieve a maximum stiffness values of 8.2 N/mm, which is higher than the bending stiffness of a plate with no perforations and no foam. In contrast, a perforation separation of 15 mm without the auxetic foam has the lowest bending stiffness (2.8 N/mm). The addition of the foam increases the bending stiffness of a plate with a perforation separation 15mm by 187 %, which is a remarkable result. When compared with a plate with a perforation separation of 10mm, the auxetic foam increases the bending stiffness by 27% only. Figure 10 shows the overall interaction between perforation dimensions and the presence of the foam. In this case the P-value of the interaction was 0.027, which is a less significant figure compared to the previous cases. One can observe some evidence that a plate with auxetic foam will produce a higher bending stiffness than a plate without. It is possible to achieve a bending stiffness higher than the plate with both no perforation and foam

lining by using a perforation separation of 35 mm with the foam. The presence of the auxetic foam on the plates increases the bending stiffness by approximately 91%.

Table 3 shows the comparison between the FE simulations and the experimental bending stiffness measured through the 3-point bending tests. A strong correlation between the experimental results and the FE simulation can be observed, with errors varying between 1.7 % and 4.9 %. The FE simulation was only performed for plates with the auxetic foam added, as this is the case that will be the most suitable for the application of torso support for comfort and tremor amplitude absorption. Figure 11 shows the stiffness map of the optimized results from the FE benchmarked models versus the variation of the perforation separation and its dimensions. Higher values of bending stiffness can be achieved with the smaller perforation dimensions and larger perforation separation. In contrast, lower values of K can be obtained with larger perforation dimensions but smaller separations. For the given configuration the optimal value of K lies within the central portion of the feasible region (20.28mm ≤ Perforation separation ≤ 30.28mm and 20.00mm≤ perforation dimension ≤40.00mm). These values of bending stiffness appear to be sufficient to provide the required support to the torso at low frequency tremors induced by MS [4].

The results shown in this work are valid for a specific thickness ratio between the foam liner and the plate (5). Different thickness ratio may and should be explored to cater for a larger design envelope. Formula (4) is related to Kirchhoff-Love plate models, and higher thickness of the support plate should be taken into account by modifications of the formula according to Mindlin plates formulations. Higher plate thicknesses should however taken into considerations with a wider variety of materials substrates, because the stiffening effect of the support may hamper the energy dissipation during dynamic loading by back reflection of the impact waves, and therefore require either a thicker padding or different designs of the support to provide the comfort typical of auxetic foams. The FE simulations made with 3D elements are however able to consider all these types of effects and shear deformations due to larger thickness values.

5. Conclusions

The paper has shown that the use of perforation patterns inducing an in-plane auxetic behaviour combined with an auxetic foam lining can provide a full auxetic structure for human body support. The hybrid composite configuration could be also further tailored to make compatible the in-plane Poisson's ratio characteristics of the plate (through the pattern of perforations) and the auxetic foam (via its manufacturing parameters). The work of this paper has focused on the optimisation of the static indentation stiffness for low-frequency tremors, however further tailoring could be performed to consider large deformation response and high-amplitude motion/vibration, because of the

unexplored effects provided by the geometry of the perforations with its stress concentration effects on the support, and the high-amplitude response of the auxetic foam. Quite significantly, the perforation technique and the type of polyurethane foam used in this design could allow using different types of material substrates, and possibly reduce the capital costs of development and increase the life cycle of the products in biomedical applications.

Acknowledgements

The work has been supported by the SARTRE (EBI) Bio-E initiative. THP acknowledges the support of the Brazilian Research Agencies (CNPq and CAPES) for the financial support provided for his stay at the University of Bristol.

Reference

[1]. http://www.mssociety.org.uk/what-is-ms/information-about-ms/about-ms (Last Accessed on 06/03/2014)
[2]. http://www.mssociety.org.uk/what-is-ms/signs-and-symptoms/tremor (Last Accessed on 06/03/2014)
[3]. M. J. Griffin. Handbook of human vibration. Academic Press Limited, 1990 London, UK.
[4]. S. H. Alusi, J. Worthington, S. Glickman, P. G. Bain, 2001. A study of tremor in multiple sclerosis. Brain 124, 720-730.
[5]. C. Geny, J.-P. Nguyen, B. Pollin, A. Feve, F. Ricolfi, P. Cesaro, J.-D. Degos, 1996. Improvement of severe postural cerebellar tremor in multiple sclerosis by chronic thalamic stimulation. Movement Disorders 11(5), 489-494.
[6]. K. L. Alderson, A. P. Pickles, P. J. Neale, K. E. Evans, 1994. Auxetic Polyethelene: the effect of a negative Poisson's ratio on hardness. Acta Metallurgica Materialia, 42(7), 2261-2266
[7]. N. Chan, K. E. Evans, 1998. Indentation resilience of conventional and auxetic foams. Cellular Plastics 34, 231-262
[8]. T-C Lim. Auxetic Materials and Structures. Springer, New York, 2015.
[9]. F Scarpa, 2008. Auxetic materials for bioprostheses. IEEE Signal Processing Magazine 25 (5), 125-126
[10]. J. P. Donoghue, K. E. Evans. Composite laminates with enhanced indentation and fracture resistance due to negative Poisson's ratio. Proc. 8th Int. Conf. on Composites Materials (ICCM8), 15th-19th July, Honolulu, Hawaii, 1991. 8K-1-10
[11]. R. S. Lakes, K. Elms, 1993. Indentability of conventional and negative Poisson's ratio foams. Journal of Composite Materials 27(12), 1193-1202
[12]. C. W. Smith, F. Lehman, R. J. Wootton, K. E. Evans, 1998. Strain dependent densification during indentation on auxetic foams. Cellular Polymers 18, 79-101
[13]. L Mizzi, D Attard, R Gatt, AA Pozniak, KW Wojciechowski, JN Grima, 2015. Influence of translational disorder on the mechanical properties of hexachiral honeycomb systems. Composites Part B: Engineering 80, 84-91
[14]. K.E. Evans, A. Alderson, 2000. Auxetic Materials: Functional Materials and structures from lateral thinking. Advanced Materials, 12 April 2000: 619
[15]. Y Liu, H Hu, 2001. A review on auxetic structures and polymeric materials. Scientific Research and Essays 5(10), 1052-1063
[16]. Gibson, L.J., Ashby, M.F., Schajer, G.S., Robertson, C.I., 2008. The mechanics of two-dimensional cellular materials, Proceedings of the Royal Society A, 382, 25-42

[17]. Masters, I.G., Evans, K.E., Models for the elastic deformation of honeycombs, Composite Structures, 35, 404-422 (1996)
[18]. J. N. Grima, R. Gatt, 2010. Perforated Sheets Exhibiting Negative Poisson's Ratios. Advanced Engineering Materials 12(6), 460-464.
[19]. T.G. Pratt. Adaptive supports for the human body. University of Bristol, MEng Report, 2011
[20]. Grima, J.N., Evans, K.E., 2000. Auxetic behaviour from rotating squares, Journal of Materials Science Letters, 19, 1563-1565
[21]. Grima J.N., Attard D., Auxetic behaviour from rotating rhombi, physica status solidi (b) 245, 2395-2404 (2008)
[22]. SIGMUND, O., 1004. MATERIALS WITH PRESCRIBED CONSTITUTIVE PARAMETERS - AN INVERSE HOMOGENIZATION PROBLEM, INTERNATIONAL JOURNAL OF SOLIDS AND STRUCTURES Volume: 31 Issue: 17 Pages: 2313-2329
[23]. SIGMUND, O., 1995. TAILORING MATERIALS WITH PRESCRIBED ELASTIC PROPERTIES, MECHANICS OF MATERIALS Volume: 20 Issue: 4 Pages: 351-368
[24]. Alderson, A., Alderson, K.L., Attard, D., Evans, K.E., Gatt, R., Grima, J.N., Miller, W., Ravirala, N., Smith, C.W., Zied, K.M., 2010. Elastic constants of 3-, 4- and 6-connected chiral and anti-chiral honeycombs subject to uniaxial in-plane loading, Composite Science and Technology, 70, 1042-1048
[25]. Scarpa, F., Blain, S., Lew, T., Perrott, D., Ruzzene, M., Yates, J.R., 2007. Elastic buckling of hexagonal chiral cell honeycomb, Composites: Part A, 38, 280-289
[26]. Gatt, R., Attard, D., Farrugia, P.S., Azzopardi, K.M., Mizzi, L., Brincat, J.P., Grima, J.N., A realistic generic model for anti-tetrachiral systems, Physica Status Solidi B, 250, 2012-2019
[27]. Pozniak, A. A., Wojciechowski, K. W., 2014. Poisson's ratio of rectangular anti-chiral structures with size dispersion of circular nodes, PHYSICA STATUS SOLIDI B-BASIC SOLID STATE PHYSICS Volume: 251 Issue: 2 Pages: 367-374
[28]. Milton, G., 1992. Composite materials with Poisson's ratios close to -1, Journal of the Mechanics and Physics of Solids, 40, 1105-1137
[29]. Strek, T., Jopek, H., Nienartowicz, M., 2015. Dynamic response of sandwich panels with auxetic cores, Physica Status Solidi B, 252, 1540-1550
[30]. Pozniak, A. A., Wojciechowski, K. W., Joseph N. Grima, Luke Mizzi, Planar auxeticity from elliptic inclusions, Composites B (in print), doi:10.1016/j.compositesb.2016.03.003
[31]. K. Bertoldi, P. M. Reis, S. Willshaw, T. Mullin, 2010. Negative Poisson's ratio behavior induced by an elastic instability. Advanced Materials 22(3), 361-366
[32]. M Bianchi, F Scarpa, CW Smith, 2010. Shape memory behaviour in auxetic foams: mechanical properties. Acta Materialia 58(3), 858-865
[33]. R Gatt, D Attard, E Manicaro, E Chetcuti, J N. Grima, 2011. On the effect of heat and solvent exposure on the microstructure properties of auxetic foams: A preliminary study. Physica Status Solidi(b), 248(1), 39-44.
[34]. A. Bezazi, F. Scarpa, 2009. Tensile fatigue of conventional and negative Poisson's ratio open cell polyurethane foams. International Journal of Fatigue 31(3), 488-494.
[35]. M. Bianchi, F. Scarpa, C. W. Smith, 2008. Stiffness and energy dissipation in polyurethane auxetic foams. Journal of Materials Science 43(17), 5851-5860
[36]. F. Scarpa, L. G. Ciffo, J. R. Yates, 2004. Dynamic properties of high structural integrity auxetic open cell foam. Smart Materials and Structures 13, 49-56
[37]. T Allen, J Shepherd, TAM Hewage, T Senior, L Foster, A Alderson, 2015. Low‐kinetic energy impact response of auxetic and conventional open‐cell polyurethane foams. Physica Status Solidi (b) 252 (7), 1631-1639
[38]. T Allen, N Martinello, D Zampieri, TAM Hewage, T Senior, L Foster, A Alderson, 2015. Auxetic Foams for Sport Safety Applications. Procedia Engineering 112, 104-109
[39]. M. Bianchi, F. Scarpa, M. Banse, C. W. Smith, 2011. Novel generation of auxetic open cell foams for curved and arbitrary shapes. Acta Materialia 59(2), 686-691

[40]. Pozniak, A. A., Smardzewski, J., Wojciechowski, K. W., 2013. Computer simulations of auxetic foams in two dimensions, SMART MATERIALS AND STRUCTURES Volume: 22 Issue: 8 Article Number: 084009
[41]. M. Bianchi, F. Scarpa. Method of Manufacturing a Foam. US Patent 8,313,682, 20 November 2012.
[42]. L Mizzi, K M. Azzopardi, D Attard, J N. Grima, R Gatt, 2015. Auxetic metamaterials exhibiting giant negative Poisson's ratios. Physica Status Solidi (RRL) - Rapid Research Letters 9(7), 425–430
[43]. S Shana, S H Kang, Z Zhao, L Fang, K Bertoldi, 2015. Design of planar isotropic negative Poisson's ratio structures. Extreme Materials Letters 4, 96-102.
[44]. A Slann, W White, F Scarpa, K Boba, I Farrow, 2015. Cellular plates with auxetic rectangular perforations. physica status solidi (b) 252 (7), 1533-1539
[45]. J. Xiong, R. Gosh, L. Ma, H. Ebrahimi, A.M.S. Hamouda, A. Vaziri, L. Wu, 2014. Bending behavior of lightweight sandwich-walled shells with pyramidal truss cores. Composite Structures 116, 793-804.
[46]. W Young, R Budynas. Roark's Formulas For Stresses and Strains. McGraw Hill Professional, New York, 2001

Figure 1

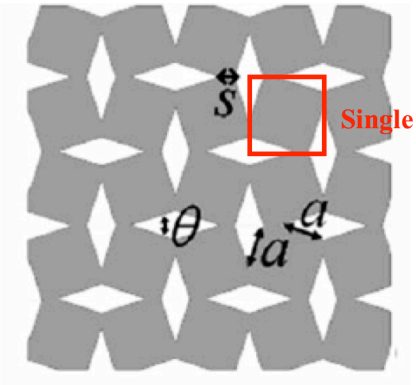

The rotating square model with variable parameters [18]

Figure 2

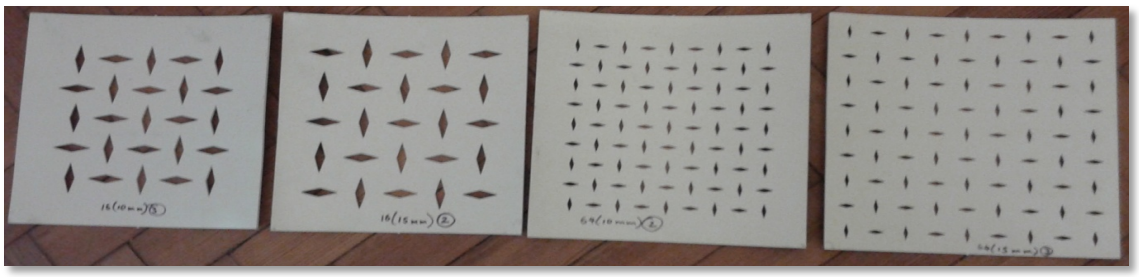

Perforated plate samples 16 C (10mm), 16 C (15mm), 64 C (10mm) and 64 C (15mm)

Figure 3

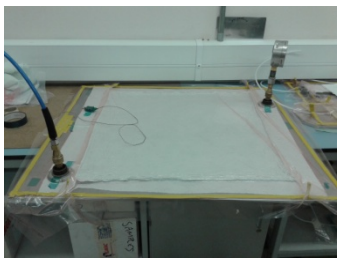

(a)

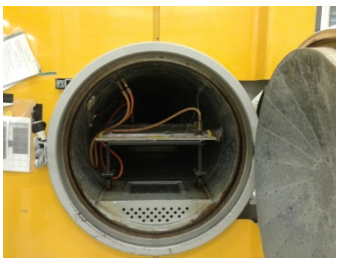

(b)

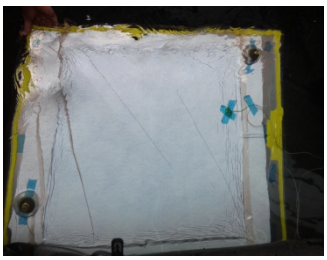

(c)

Phases of the fabrication of the auxetic foam pad. (a) Vacuum-bagging and positioning of the pumps; (b) bagged foam with thermocouples in the autoclave; (b) release of the cooled foam

Figure 4

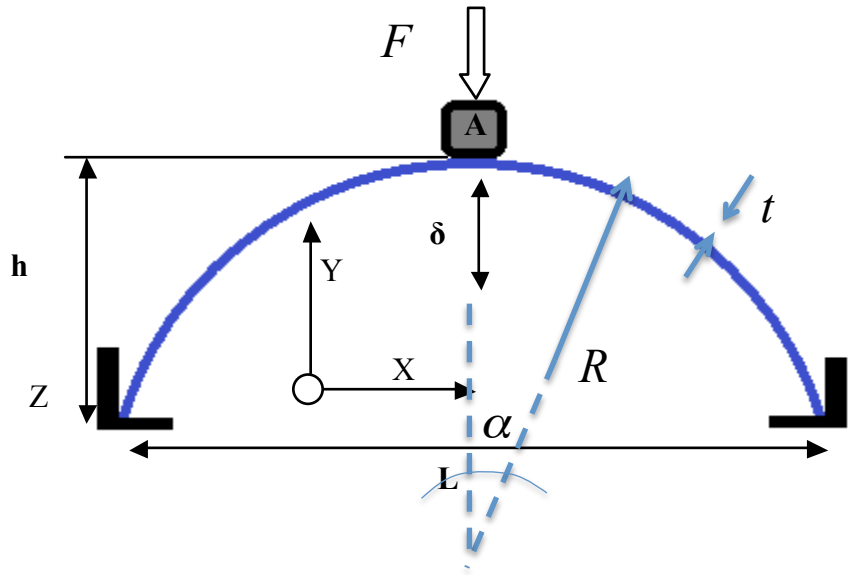

Schematic view of the analytical model of the curved plate.

Figure 5

(a) **(b)**

Three-point bending tests for (a) the flat nylon and (b) curved plate with the auxetic foam layer

Figure 6

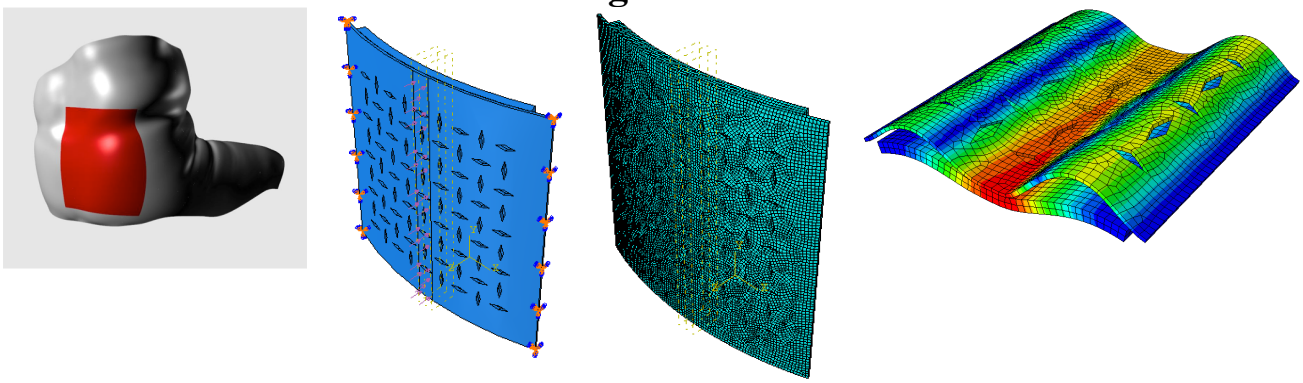

(a) (b) (c) (d)

(a) Possible location of a low-back hybrid auxetic support. (b) Solid model representing a perforated plate with the foam liner in 3-point bending and (c) its Finite Element representation. (d) FE deformation under 3-point bending boundary conditions. The foam liner has been separated from the perforated support to show the deformation field.

Figure 7

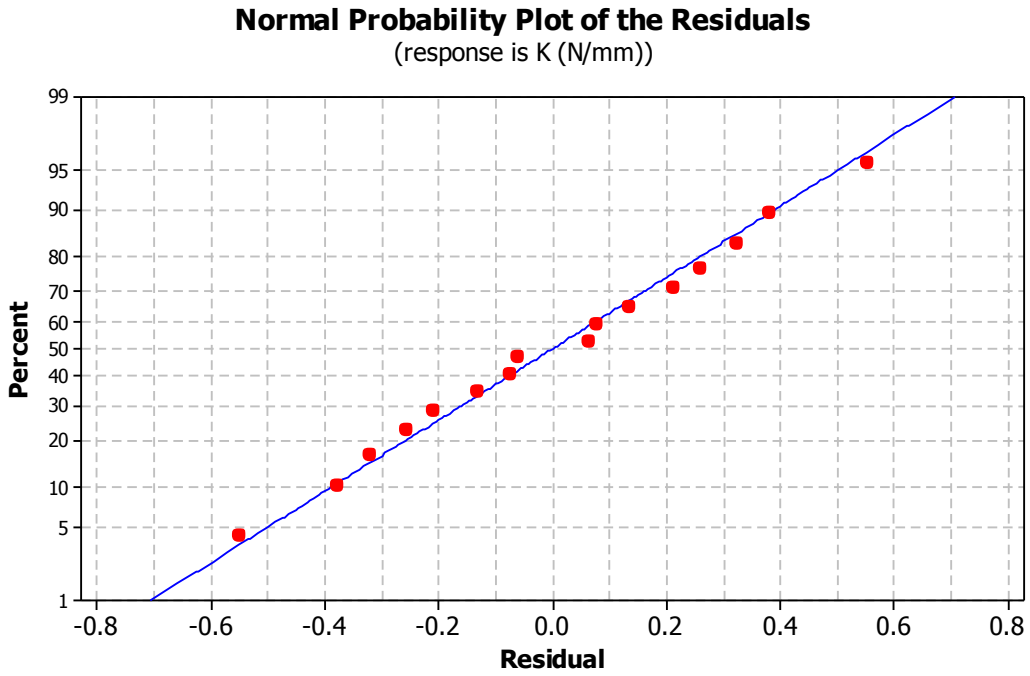

Normal probability distribution of the experimental results

Figure 8

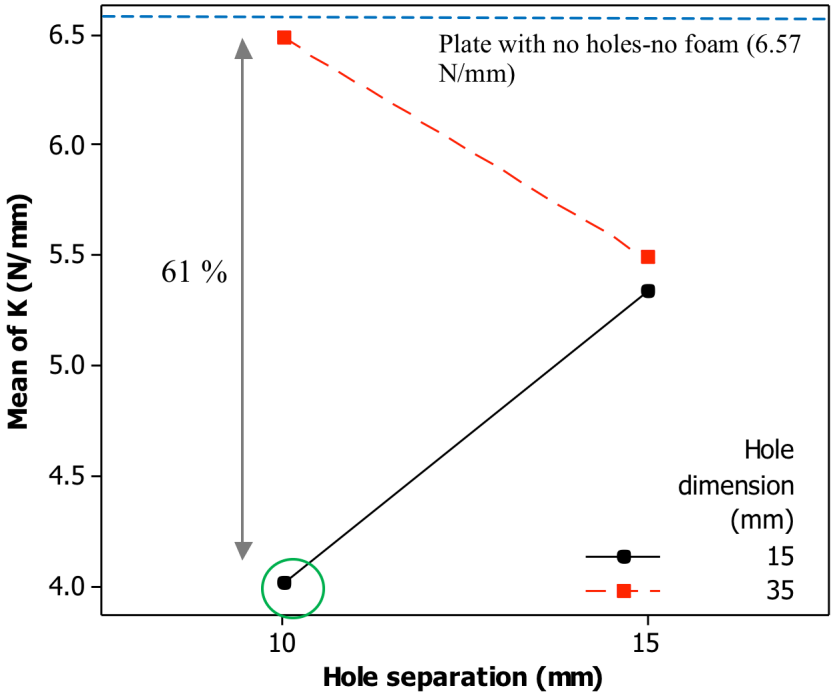

Interaction between the dimensions and the separation distance of the perforations

Figure 9

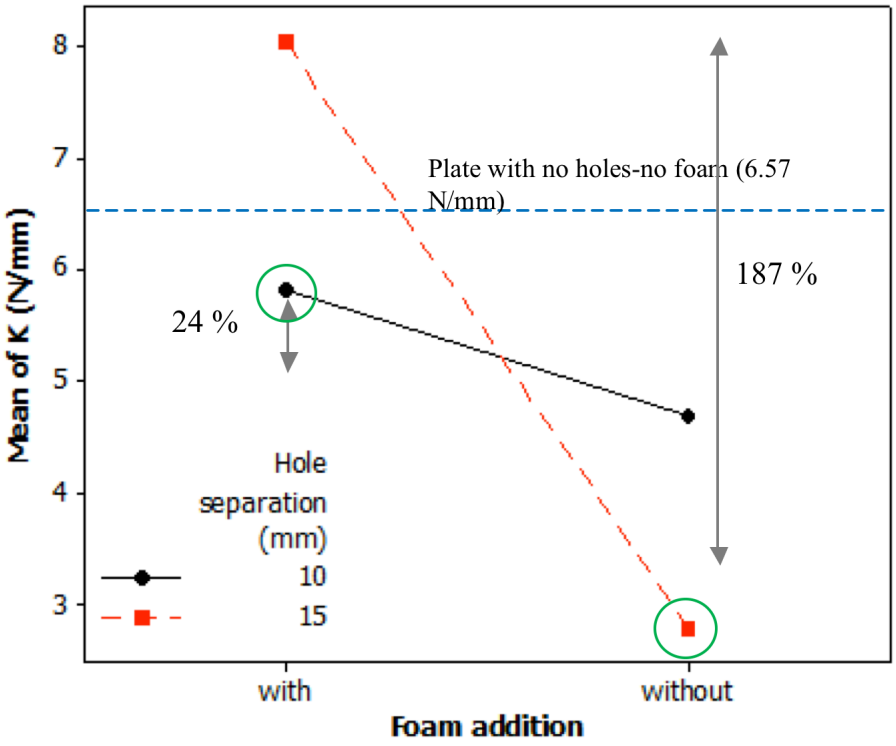

Interaction between hole separation and the presence of the foam layer. Hole dimension of 35 mm.

Figure 10

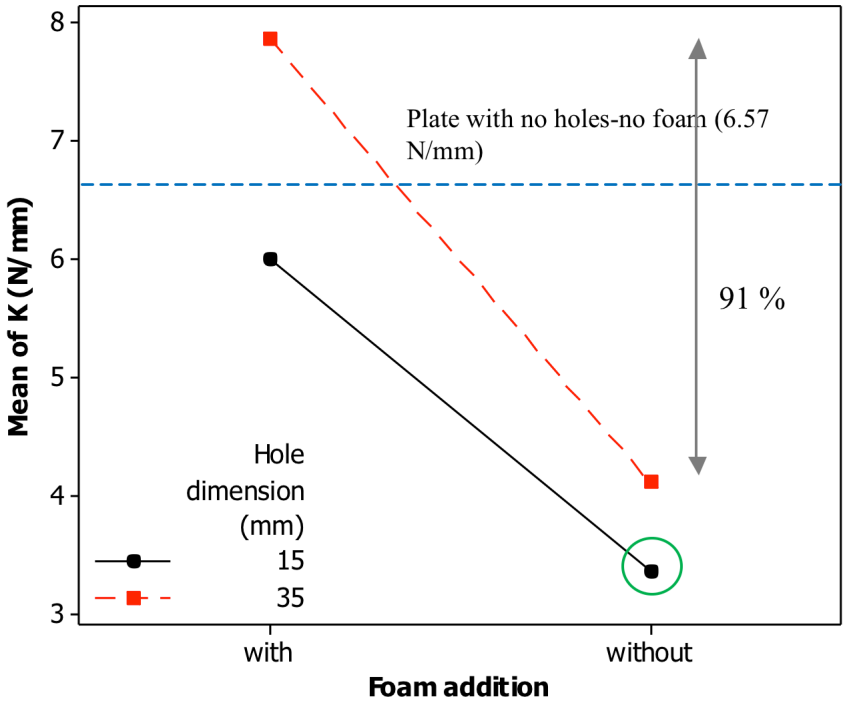

Effect of the interaction between hole dimensions and presence of the foam over the radial stiffness of the plates. Hole spacing of 15 mm.

Figure 11

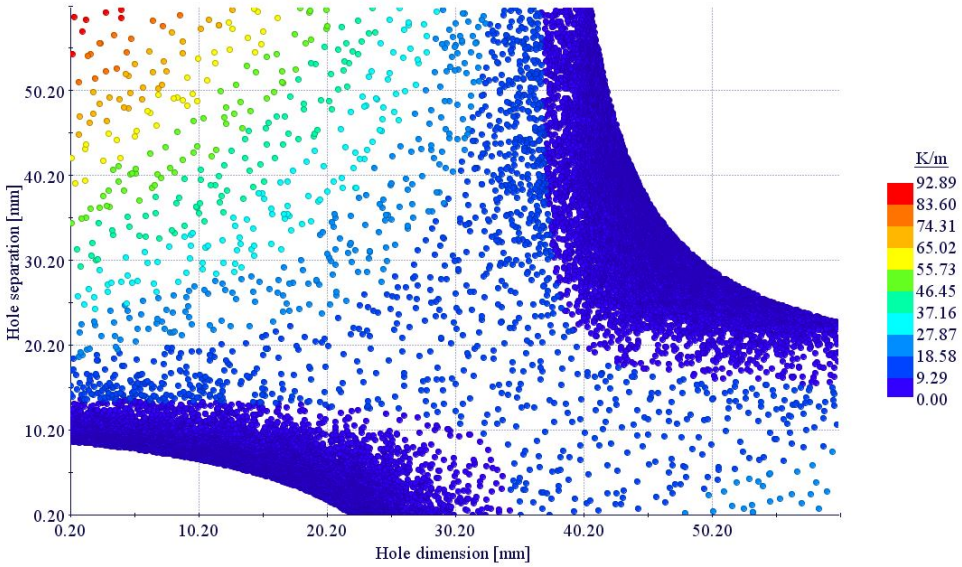

Map of the optimal values of the radial stiffness *K* versus the geometry of the rhomboidal perforations via the FE-based optimization.

Table 1

Sample Name	Perforation Density/Cell number	Perforation Separation s (mm)	Perforation Dimension (mm)
1	16	10	35
2	16	15	35
3	64	10	15
4	64	15	15

Table 1. Dimensions and geometry properties of the auxetic perforated plates manufactured in this work

Table 2

	Analysis of Variance (ANOVA)– Design of Experiment (2^3)		
	Factors	**F**	**P-value ≤ 0.05**
Main Factors	Hole dimension	39.66	0.000
	Hole separation	0.62	0.455
	Foam addition	235.36	0.000
Interaction of factors	Hole dimension*Hole separation	31.14	**0.001**
	Hole dimension*Foam addition	7.35	**0.027**
	Hole separation*Foam addition	97.44	**0.000**
	Hole dimension*Hole separation* Foam addition	0.71	0.423
	S = 0.415829 R-Sq = 98.10%		

Table 2. Analysis of variance of the different experimental factors.

Table 3

Sample Nº	Perforation Dimension [mm]	Perforation Separation [mm]	Experimental values *K* [N/mm]	Predicted values *K* [N/mm]	Percentage Error (%)
1	35	10	7.80	7.42	4.87
2	35	15	8.63	8.30	3.75
3	15	10	4.42	4.21	4.74
4	15	15	7.90	7.77	1.68

Table 3. Comparison between FE and experimental values of radial stiffness for the auxetic perforated plates with the NPR foam liners.